Intensity Calibration and Sensitivity Comparisons for CCD/Raman Spectrometers

MARK FRYLING, CHRISTOPHER J. FRANK, and RICHARD L. McCREERY*
Department of Chemistry, The Ohio State University, 120 West 18th Avenue, Columbus, Ohio 43210

A calibrated tungsten source combined with a fiber optic was used to correct Raman spectra for instrumental response. With the placement of the fiber output at the Raman sample position, the product of throughput, collection efficiency, quantum efficiency, and sampled area could be assessed. This product is related to a spectrometer figure of merit, which provides a quantitative comparison of spectrometer sensitivity and signal-to-noise ratio. Four spectrometer configurations were compared to illustrate the approach. An additional feature of the white light calibration is correction of relative Raman peak intensities. This issue is particularly important due to the substantial differences between CCD quantum efficiency curves and those of photomultipliers or intensified photodiode arrays.

Index Headings: **Raman; Multichannel; CCD; Array detectors; Calibration.**

INTRODUCTION

The widespread use of array detectors in Raman spectroscopy started with vidicons and diode arrays[1,2] and continued with charge-coupled devices (CCDs).[3-6] The merits of multichannel detectors for dispersive Raman spectroscopy have been discussed on several occasions.[7-12] Array detectors have yielded major improvements in signal-to-noise ratio (SNR) or decreased measurement time or both, and in many cases permit observations which were not possible with single-channel photomultiplier (PMT) spectrometers. The use of silicon as the photosensitive element in CCDs permits operation in the NIR region with 632–830 nm lasers, thus reducing fluorescence interference.[5,13-17] In addition, cooled CCDs can exhibit very low background signals, often $<0.1\ e^-$/min, so that dark and readout noise are insignificant in comparison with sample shot noise. The advantages of sensitivity, NIR operation, low noise, and multichannel operation have made CCD Raman spectrometers very attractive when compared to scanning PMT systems. In addition, the operation of multichannel CCD systems in the shot noise limit often leads to significantly lower detection limits than FT-Raman, often at quite low laser powers. There is every indication that CCD Raman spectrometry will become a routine alternative to FT-Raman and single-channel techniques.

Raman spectroscopy with multichannel CCD detectors brings with it several issues of calibration and instrumental technique. First, wavelength accuracy is usually poorer than that for FT or scanning systems, due to variable detector position and nonlinearity across a wide (2.5-cm) flat field, so that the Raman shift scale must be calibrated.[18,19] Second, each detection element of a CCD is generally smaller than that of a PMT, but larger than a diode array element. Although this consideration results in some loss of collection efficiency and often affects spectrometer design, it is compensated for by the multichannel advantage.[7] Third, the quantum efficiency curve (Q) for a silicon CCD is quite different from that for a typical PMT, leading to relative intensity changes which are significant but correctable. Fourth, CCDs are often used with laser rejection filters, which contribute to the instrument response function.[14,20] It is desirable to calibrate the filter transmission, spectrograph throughput, and detector Q with a known continuum source. Fifth, collection efficiency depends on input optics, $f/$, and detector area, which may be quite different for the single and triple spectrographs used with CCDs, in comparison to the double/PMT case.[7,12] Finally, the detector noise of a CCD is usually negligible in comparison with sample shot noise, allowing long integration times, in contrast to the use of a diode array or PMT. This fact modifies the signal-to-noise ratio equations and ultimately the experimental design.

Design parameters for signal and SNR optimization have been considered in both recent[7,12,21-24] and older[25-28] literature. Hamaguchi reviewed several issues of wavelength and sensitivity calibration for array detectors used in Raman,[19] and Shen *et al.* have pointed out the importance of accurate wavelength calibration.[18] Strommen and Nakamoto have reviewed several calibration procedures which predate the use of CCDs.[29] Given the rapid evolution of CCD-based Raman spectrometers, it is important to reconsider past treatments in light of technological developments.

Received 22 June 1993.
* Author to whom correspondence should be sent.

0003-7028/93/4712-1965$2.00/0
© 1993 Society for Applied Spectroscopy

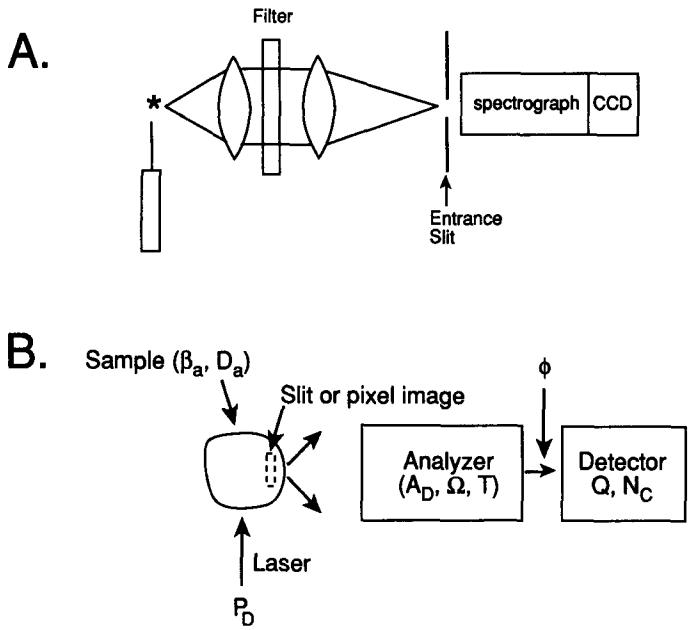

FIG. 1. (A) Generic Raman spectrometer upon which theoretical expressions are developed, shown for the case of 90° light collection. (B) Representation of variables involved in quantifying Raman signal.

The work reported herein was undertaken to illustrate and optimize the factors affecting performance of multichannel CCD Raman spectrometers. After a theoretical discussion of the dependence of signal and SNR on various experimental parameters, examples of several relevant spectral measurements are presented. In particular, a standard white source was used to evaluate spectrograph throughput and collection efficiency and correct spectra for the instrument response function. The operations are illustrated for several CCD Raman spectra under a variety of experimental conditions.

THEORY

Before particular experimental issues are considered, theoretical expressions relating response to sample and spectrometer variables are necessary. The following treatment is a more specific and detailed version of that reviewed previously.[12] Any Raman experiment is characterized by a rather large number of experimental variables, so that it is difficult to derive a universally applicable expression for signal (S, photoelectrons) or SNR. Much of the difficulty arises from the need to map a two- or three-dimensional scattering volume onto a two-dimensional detector, with intervening collection lenses, filters, and spectrographs. There are many parameters—such as the size of the scattering volume relative to the slit, the linewidth of the Raman line relative to the spectral bandpass, the pixel width relative to the slit width, etc.—which vary from instrument to instrument and which have a profound effect on S or SNR. The present discussion is limited to dispersive Raman with one of several illumination and collection geometries. The generic apparatus is that of Fig. 1A, with collection optics, filters, spectrograph, and detector. The detector noise is assumed to be negligible in all cases, so that the only noise source is shot noise from the sample, both analyte and background. Background is defined as any laser-derived light other than analyte Raman, and includes stray light, solvent Raman, and sample luminescence. Unless stated otherwise, the sample scattering *overfills* the spectrometer, meaning that the image of the scattering volume at the entrance slit is larger than the slit itself, *and* the solid angle of scattering is larger than the solid angle collected. This arrangement maximizes the signal by using all the available detector or slit area. Fifth, the Raman scattering will be considered to be linear with laser power and *isotropic*. Although scattering from polarized bands in liquids or most crystals is nonisotropic, the assumption avoids the dependence of cross section on geometry, and will be valid for liquids observed in backscattered geometry and many other common situations. If the cross section is considered nonisotropic, the effect is a variation in cross section with geometry, thus introducing an additional factor into the S and SNR expressions. Finally, we will assume that the power density of the laser at the sample is constant both across the beam and along the propagation axis. This assumption precludes consideration of absorbing samples in the present discussion, and ignores the Gaussian shape of the beam cross section.

The instrument is conveniently divided into three distinct components for purposes of relating S and SNR to instrumental parameters,[8] with reference to Fig. 1B. First, the sample has a characteristic specific intensity, L, with units of photons s^{-1} cm^{-2} sr^{-1}. L is the total Raman scattering divided by the area of the scattering volume. L is governed by Eq. 1:

$$L = P_D\left(\frac{d\sigma}{d\Omega}\right)_a D_a K \qquad (1)$$

where P_D = laser power density (photons s^{-1} cm^{-2}); $d\sigma/d\Omega$ = analyte differential Raman cross section (cm^2 molecule^{-1} sr^{-1}); and D_a = analyte number density (molecules cm^{-3} for liquids). The expression $d\sigma/d\Omega$ will be denoted β_a henceforth for convenience. Note that β_a is integrated with respect to wavelength over the entire Raman linewidth, and therefore a Raman signal calculated from β represents the integral of the signal over the Raman linewidth. K is a constant which will be defined later for different geometries. (See Table I for a complete listing of mathematical expressions.)

The second general instrumental component is the collection optics and spectrograph. This system collects some solid angle Ω and some area A_D from the scattering volume. Note that A_D is the sample area actually collected by the spectrograph. It is usually the entrance slit image *at the sample,* perhaps demagnified from the actual slit area. For cases where the spectrometer is *underfilled,* A_D is the area of the sample volume monitored by the spectrometer (e.g., the beam waist region). The photon flux Φ (photons s^{-1}) leaving the spectrograph is given by Eq. 2:

$$\Phi = LA_D T(\lambda)\Omega \qquad (2)$$

where: L = specific intensity at sample (photons s^{-1} cm^{-2} sr^{-1}); A_D = area of sample monitored by spectrograph—usually the slit image (cm^2); $T(\lambda)$ = transmission of spec-

trograph, collection optics, and filters (unitless); and Ω = collection angle *at the sample* (sr).

Note that the $A_D\Omega$ product (often called *etendue*) remains constant through the spectrograph and collection optics, even if magnification occurs. For a well-designed system, the $A_D\Omega$ product is determined by the detector area and the spectrograph *f*/ (which determines Ω), provided that the spectrograph is overfilled. The treatment thus far is analogous to that of Schrader *et al.*[22] for FT-Raman systems, and in both cases Φ is a product of L at the sample and spectrograph parameters $A_D\Omega T$.

The third major component is the detector, whether single or multichannel. Considering single-channel performance for the moment, the Raman signal is given by Eq. 3:

$$S \text{ (photoelectrons)} = \Phi Q(\lambda)t \tag{3}$$

where $Q(\lambda)$ = quantum efficiency (photoelectrons photon^{-1}); and t = measurement time (s). In the case of CCDs, the A/D output is easily converted to photo-electrons by a known gain factor. It is sometimes the case that the entrance slit is wider than a single CCD pixel; in this case, the A_D in Eq. 2 is the *pixel* image at the sample and S is for each pixel. Alternatively, if A_D is the *slit* image, then S is the sum of the electrons in the pixels contained within the slit image. In the unusual case that the slit image is narrower than the pixel, A_D is determined by the slit.

The noise characteristics of the detector are not relevant to the magnitude of the signal and are usually negligible for a liquid nitrogen-cooled CCD. This property is a major advantage of CCDs over intensified diode arrays and PMTs,[4,12] particularly for weak signals. The multichannel advantage will be considered later, and the discussion thus far treats only one channel of a CCD array. Combination of Eqs. 1–3 yields:

$$S = P_D\beta_A D_a\Omega TQA_D Kt. \tag{4}$$

Sampling Geometries. The relationship between the input laser beam and collection optics determines K. Functionally, K relates L to sample and laser parameters, via Eq. 5:

$$K = \frac{L}{P_D\beta_a D_a} \tag{5}$$

and is essentially the scattering volume divided by the scattering area. It is best appreciated by considering several common cases.

Case 1: 90° Collection from Transparent Samples. For this case (see Fig. 2), L equals the total Raman scattering from the sampled volume divided by the area of the scattering cylinder:

$$L = \frac{P_D\beta_a D_a\pi a^2 d}{2a\pi d} = P_D\beta_a D_a\left(\frac{a}{2}\right) \tag{6}$$

so $K = a/2$, and S is given by Eq. 4. Signal can also be expressed in terms of power (P_0, photons s^{-1}) rather than power density, yielding $K = 1/2\pi a$ and:

$$S = \frac{P_0\beta_a D_a\Omega A_D TQt}{2\pi a}. \tag{7}$$

TABLE I. List of symbols and units.

a	Beam radius at sample, cm
A_D	Sample area monitored by spectrograph, cm^2
A_F	Area of fiber end monitored by spectrometer
β_a	Cross section of analyte (often denoted $d\sigma/d\Omega$), cm^2 molecule^{-1} sr^{-1}
β_B	Cross section of background process
β_s	Cross section of a molecule on a surface, cm^2 molecule^{-1} sr^{-1}
D_a	Number density of analyte, molecules cm^{-3}
D_B	Number density of background, molecules cm^{-3}
D_E	Number density of analyte on a surface, molecules cm^{-2}
d	Laser pathlength monitored by spectrometer, cm
$\Delta\lambda$	Bandpass of spectrometer, nm
F_s	Spectrometer figure of merit, based on signal, sr cm^3 e$^-$ photon^{-1}
F_{SNR}	Spectrometer figure of merit, based on SNR, sr$^{1/2}$ cm$^{3/2}$ $e^{1/2}$ photon$^{-1/2}$
$I(\lambda)$	Irradiance of standard source at 100 cm, photons s^{-1} cm^{-2} nm^{-1}
K	Geometric factor, usually in cm
L	Specific intensity (often called radiance), photons s^{-1} cm^{-2} sr^{-1}
L_F	Specifc intensity of white light fiber, photons s^{-1} cm^{-2} sr^{-1} nm^{-1}
N_C	Number of pixels along the wavelength axis of a CCD
N_R	Number of resolution elements for a given spectrum
Ω	Collection angle of spectrometer, measured at the sample, sr
P_D	Laser power density, photons s^{-1} cm^{-2}
P_o	Laser power, photons s^{-1}
Φ	Photon flux leaving spectrograph, photons/s
Q	Detector quantum efficiency, photoelectrons photon^{-1}
r_F	Radius of white light fiber, cm
r_s	Radius of fiber output cone at slit, cm
S	Signal measured at CCD, electrons
$S_s(\lambda)$	Spectrum of standard source at 100 cm, e^-
S_{corr}	Spectrum of a sample corrected for instrumental response, e^-
S_{obs}	Observed sample spectrum before correction, e^-
t	Measurement time, s
T	Spectrometer transmission, unitless

Note that for Eq. 4, a smaller beam radius *decreases* the value of S, since a constant power density illuminates fewer scatterers. From Eq. 7, smaller beam radius *increases* the value of S, since the same power is illuminating a smaller region, increasing P_D and L. For both cases recall that the spectrometer is *overfilled*. If the slit area were *underfilled*, Eq. 8 would result:

$$S = \frac{P_0\beta_a D_a d\Omega TQt}{\pi}. \tag{8}$$

For this case, the image of the slit at the sample is larger than the beam width, and A_D equals $2ad$. Provided that the slit is underfilled, laser beam radius does not affect S.

Case 2: Scattering from a Surface. Slight modification of Eqs. 1 and 4 is required since the scatterer number density is now molecules cm^{-2}. If D_s = surface number density of scatterers,

$$L = P_D D_S\beta_s. \tag{9}$$

Note that $K = 1$. For an overfilled slit (Fig. 3A):

$$S = P_D\beta_s D_s\Omega A_D TQt. \tag{10}$$

Changes in the incidence angle of the laser will change P_D. For an underfilled slit and 180° geometry (Fig. 3B),

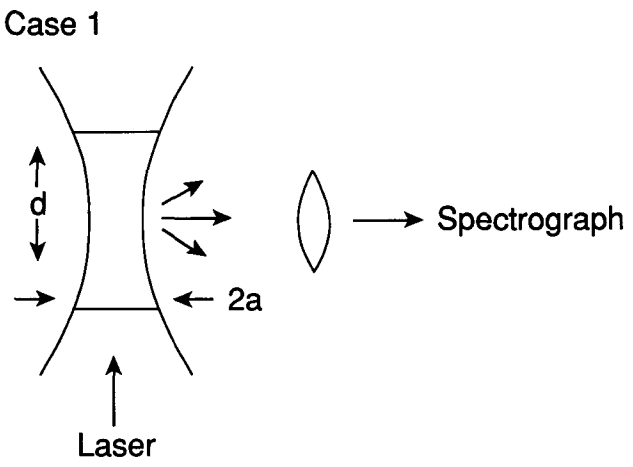

FIG. 2. The 90° geometry, referred to as Case 1 in the text. The sampled volume is defined by a cylinder of diameter $2a$ and length d.

the size of the focal spot has no effect on S, since $A_D = \pi a^2$:

$$S = P_0 \beta_a D_s \Omega T Q t. \quad (11)$$

Signal-to-Noise Ratio. As noted earlier, the dark noise and readout noise of a modern cooled CCD detector are usually much smaller than the sample shot noise. In addition, variations in laser intensity with time do not cause noise in the spectrum, since the entire spectral range is monitored simultaneously with an array detector. Thus CCD Raman spectrometers generally yield a situation where the only noise source is sample shot noise from both analyte and background scatter. Background scattering is governed by relationships similar to those for analyte Raman (e.g., Eq. 4), except that we will combine all background scatter (regardless of origin) into a single term with a cross section β_B and number density D_B.

When the SNR is determined solely by analyte or background shot noise, it is relatively simple to predict how the SNR depends on experimental variables. The signal is taken as the mean peak height above the background, and the noise is the square root of the total (analyte + background) signal. Applying this analysis to Eq. 4 yields:

$$\mathrm{SNR} = \frac{\beta_a D_a}{(\beta_a D_a + \beta_B D_B)^{1/2}} (P_D \Omega A_D T Q t K)^{1/2}. \quad (12)$$

Note that the SNR is linear in $\beta_a D_a$ if background scattering dominates, while SNR is linear in $(\beta_a D_a)^{1/2}$ if background scattering is negligible.

A CCD array with N_c pixels along the wavelength axis provides a multichannel advantage relative to a scanning PMT system. The slit image might overlap more than one pixel, yielding N_R resolution elements with $N_R \leq N_c$. A multichannel system can monitor each resolution element N_R times longer than a scanning instrument for the same total measurement time. Thus t in Eq. 12 is replaced with $N_R t$, with $N_R = 1$ for a PMT, and up to 1152 or more for currently available CCDs:

$$\mathrm{SNR} = \frac{\beta_a D_a}{(\beta_a D_a + \beta_B D_B)^{1/2}} (P_D \Omega A_D T Q K N_R t)^{1/2}. \quad (13)$$

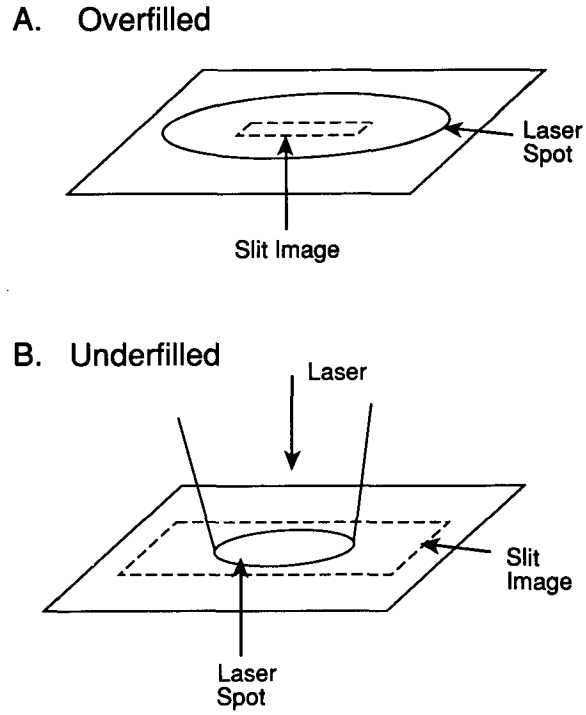

FIG. 3. The 180° backscattering geometry applied to the solid surface, showing two limiting cases for the relative size of laser focus and slit image.

Recall that t is the measurement time for each resolution element of a single channel instrument, and $N_R t$ is the measurement time for each pixel of a multichannel system. The familiar $N_R^{1/2}$ multichannel advantage is the SNR improvement for a multichannel system relative to a single channel *provided that all else is equal* (i.e., A_D, Q, etc.). The CCD gain (ADU/photoelectron) does not affect the SNR provided that it is constant and does not introduce quantization noise.

A simple but useful modification of Eq. 4 provides a spectrometer figure of merit (F_s) which permits comparisons of spectrometer sensitivity:

$$F_s = \frac{S}{\beta_a D_a P_D t} = \Omega A_D T Q K. \quad (14)$$

This rearrangement separates sample and laser variables from spectrometer variables, since the left side depends only on sample concentration, identity, and laser variables. By comparing S for a given $(\beta_a D_a P_D t)$ product, one can assess the relative sensitivities of different spectrometers. One is essentially comparing the $(\Omega A_D T Q K)$ product for different systems. Similar expressions are available for SNR for the case where a multichannel spectrum is acquired for $N_R t$ seconds compared to t seconds for each resolution element of a scanning system. In the analyte shot noise limit:

$$F_{\mathrm{SNR}} = \frac{\mathrm{SNR}}{(\beta_a D_a P_D t)^{1/2}} = (\Omega A_D T Q N_R K)^{1/2}. \quad (15)$$

A more efficient spectrometer will have a higher F_{SNR} and

TABLE II. Spectrograph configurations.

Label	Collection/ spectrometer f/[a]	Spectrometer	Grating 1/mm and blaze (dispersion cm^{-1}/mm)	Detector	Relative F_s (600 nm)[b]	Relative F_s (800 nm)[b]
A	1/8	Spex 1403 double monochomator	1800/450 nm (12.5)[c]	RCA 31034A PMT	1.0	0.38
B	4/5.6	ISA 640 mm single spectrograph	150/500 nm (148)[c]	PM512 CCD 512 channels	1.67	0.55
C	4/5.6	ISA 640 mm single spectrograph	300/l μm (76)[d]	EEV05-10 CCD 1152 channels	0.53	0.99
D	4/4	Chromex 250 mm single spectrograph	300/l μm (187)[d]	TEK 512 CB/AR 512 channels back-thinned and AR coated	3.14	4.73

[a] First number is f/ of collection optics, second is f/ of spectrometer.
[b] For 1 cm^{-1} resolution.
[c] Dispersion was calculated at 514.5 nm.
[d] Dispersion was calculated at 800 nm.

$\Omega A_D TQN_R K$ product, yielding a higher SNR for a given $\beta_a D_a P_D t$; in addition, SNR will scale with $\beta_a^{1/2}$, $D_a^{1/2}$, and $t^{1/2}$ for a given F_{SNR}.

Some additional practical considerations of CCD detectors deserve note at this point. First, a larger A_D improves S and SNR since a larger number of scatterers are monitored. However, if A_D is increased by increasing the slit width, then N_R is decreased once the slit width exceeds the pixel width. There is a trade-off of A_D and N_R which is fundamental to array detectors. A second but related issue is the matching of A_D to the detector element size. With relatively large PMT detectors (~2 × 20 mm), it is common to increase Ω at the sample by decreasing A_D, a process usually called f/ matching. For example, a ~100-μm beam waist can be magnified to match a 1-mm slit width, in the process matching f/1 collection optics to an f/10 spectrometer. Since CCD pixels and associated entrance slit are relatively narrow (typically 20–25 μm for pixel width, 20–100 μm for typical slit widths), f/ matching is of little value. If the spectrograph is overfilled, as is usually the case for CCD systems, $A_D\Omega$ is constant and increasing Ω by f/ matching will only decrease A_D, leading to no gain.[7] We have found that keeping the collection optics f/ approximately equal to that of the spectrograph is both convenient and effective for CCD systems. A third practical issue is the relationship of L to P_D. Increasing L always improves S and SNR, but power density is ultimately limited by sample radiation damage. This is a particular concern with microprobes, where P_D can be 10^2–10^3 times higher than that for conventional systems. In practical terms, S and SNR are often limited by the detector area and spectrograph f/ (through $A_D\Omega$) and by the maximum power density imposed by sample radiation damage.

EXPERIMENTAL

The Raman spectrometers employed are listed in Table II. The Spex 1403 was equipped with a Model 1459 sample chamber which f/ matches an f/1 elliptical collector to an f/8 monochromator. The entrance optics on the ISA systems employed 120-mm, f/4 lenses, while the Chromex Raman One has built-in collection optics and filter holders (f/4). Laser sources were either a Coherent 70-5 Ar^+ laser or a Coherent Ti:sapphire laser pumped by a Coherent 90-5 Ar^+ laser (5 W all lines). In all cases, laser output was filtered by an interference filter ("DF10" series, Omega Optical, Brattleboro, VT). The cooled PMT (RCA 31034A) had a dark signal of 4 counts/s, and the CCDs were all cooled to −110°C. CCD spectra were bias corrected and multiplied by CCD gain (e^-/ADU), but dark subtraction was unnecessary for the short integration times employed. The standard irradiance source (Eppley Labs, Newport, RI) was calibrated by the manufacturer against NIST standards at 31 wavelengths in the 250–2400 nm range and was directed through a diffuser into a 200-μm optical fiber cable from C-Technologies (Verona, NJ). The output cone of the fiber was approximately f/1.8, which overfills the collection angle of all but spectrometer A.

The Raman shift axis of CCD spectra was calibrated by a second-order fit to known band positions of naphthalene or indene. All samples were reagent-grade chemicals, except for the oleic acid methyl ester obtained from Sigma.

RESULTS

Since grating efficiency, detector Q, and filter transmission all vary significantly with wavelength, it is useful to correct observed spectra for the overall instrument response function. Previous reports discuss the use of a white source, often tungsten, which is recorded under the conditions used for Raman spectral acquisition.[14,29] If the white output is assumed to be constant with wavelength over the relevant range, the spectrum of the tungsten source is then divided into the observed Raman spectrum to correct for instrument response. A more accurate procedure employs a calibrated white source or blackbody radiator whose output (photons $s^{-1}\,cm^{-2}\,nm^{-1}$) is known to <5% accuracy over the relevant wavelength range. This approach still falls short of ideal, however, since the white source is usually not placed at the Raman sample position and does not follow the same path through the optics. If a standard irradiance source (or even a nonstandard flashlight) is placed some distance away from the sample position, the spectrometer is collecting nearly collimated light, which is not representative of the Raman experiment. An ideal calibration source would be a weak white source with known specific in-

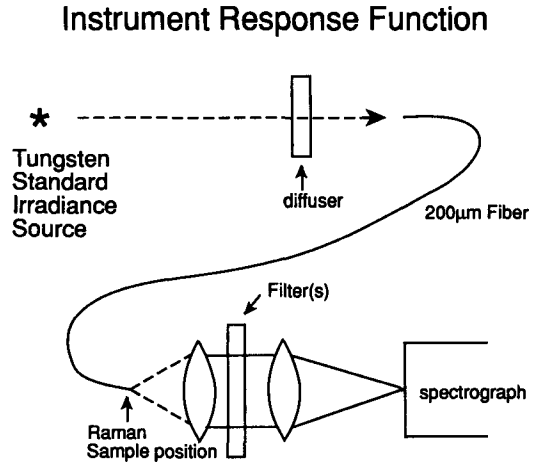

FIG. 4. Apparatus for generating white light emission from the end of an optical fiber.

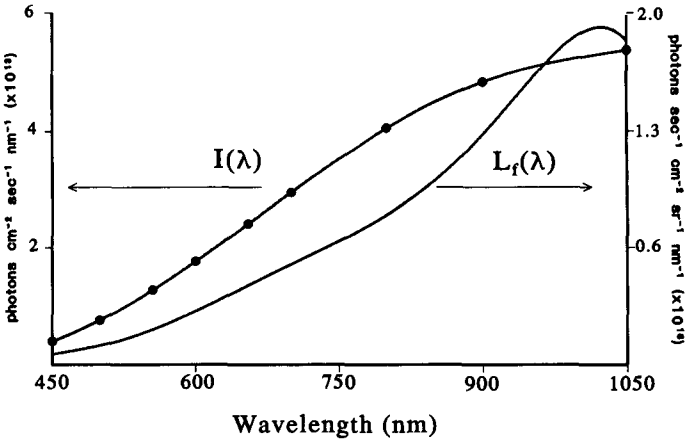

FIG. 5. Irradiance of standard source ($I(\lambda)$) and specific intensity of fiber output. Points indicate manufacturers' values for irradiance; the $I(\lambda)$ line is a fifth-order polynomial fit to the points. $L_F(\lambda)$ was determined as described in the text.

tensity placed at the sample position and comparable in size to the Raman scattering area.

Such a calibration source is approximated by the apparatus in Fig. 4, in which a 200-μm fiber carries a standard source output to the Raman sample position. After the determination of the shape of the fiber output as specific intensity as a function of wavelength, $L_F(\lambda)$ (photons s^{-1} cm^{-2} sr^{-1} nm^{-1}), the fiber becomes a secondary standard which mimics a Raman sample with known specific intensity. In effect the fiber has converted a known irradiance source into a specific intensity standard which fills the spectrometer collection optics. To determine $L_F(\lambda)$, we used spectrograph **B** to compare the known standard irradiance curve from the source manufacturer ($I(\lambda)$) to the fiber output. A spectrum ($S_s(\lambda)$) was first recorded with the tungsten source 100 cm away from the entrance slit, and no intervening optics. The known $I(\lambda)$ under these conditions is shown in Fig. 5. After inserting the diffuser and fiber and placing the fiber ~1 cm away from the entrance slit, we recorded the spectrum again ($S_F(\lambda)$). $L_F(\lambda)$ was then determined by Eq. 16:

$$L_F(\lambda) = \frac{I(\lambda)}{\Omega}\frac{S_F(\lambda)}{S_s(\lambda)}\frac{r_s^2}{r_F^2}. \tag{16}$$

The spectrometer Ω occurs in Eq. 16 because the exit cone from the fiber now overfills the spectrometer acceptance angle. The factor of r_s^2/r_F^2 accounts for the expansion of the fiber output cone from the fiber radius (r_F) to the radius at the slit (r_s), and equals 772 in this case. The resulting $L_F(\lambda)$ is also shown in Fig. 5, with the difference in shape from $I(\lambda)$ attributable mainly to fiber transmission variation with λ. Although the absolute magnitude of $L_F(\lambda)$ obtained by this procedure should be considered approximate due to uncertainties in Ω and the fiber output cone geometry, its *shape* is much more reliable. As long as the sources of error are only very weakly dependent on λ, the procedure yields an accurate shape for the $L_F(\lambda)$ curve, and a magnitude which is precisely reproducible if not accurately known in absolute terms.

With the entrance optics of the spectrometer in place for a Raman experiment, the white light fiber is placed at the sample location and positioned for maximum response. By analogy to Eqs. 2 and 3, the signal under these conditions is:

$$S_F = L_F\Omega T(\lambda)Q(\lambda)A_F t\Delta\lambda. \tag{17}$$

Note that A_F is the fiber cross section monitored by the spectrometer (with any magnification taken into account). $\Delta\lambda$ is included because the source is white; $\Delta\lambda$ equals the reciprocal linear dispersion times the slit width (or pixel width).

With the calibrated fiber in place, it is possible to calculate the function ΩQT via Eq. 18:

$$\Omega T(\lambda)Q(\lambda) = \frac{S_F}{L_F t\Delta\lambda A_F}. \tag{18}$$

Finally, the function ΩTQA_D may be determined for a Raman experiment provided that the area (A_D) of the Raman scattering volume monitored by the spectrometer is known. ΩTQA_D provides a quantitative comparison of spectrometer sensitivity, and indicates the signal observed for a given sample and collection geometry. It is proportional to the figure of merit defined in Eqs. 14 and 15. In practice, the ΩTQA_D product is determined by monitoring S_F for a given configuration, calculating ΩTQ,

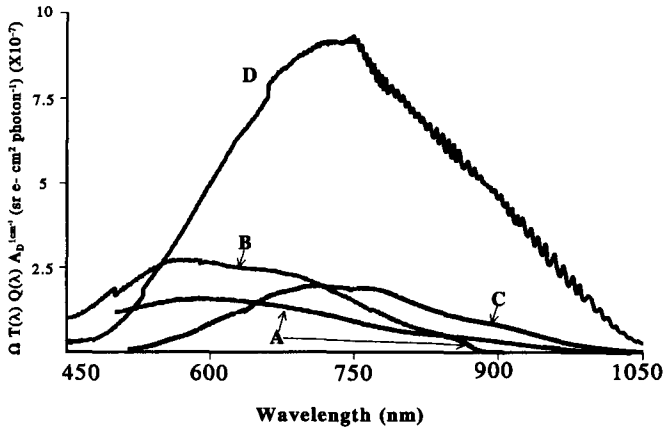

FIG. 6. Response curves for spectrometers listed in Table I, all adjusted to a theoretical bandpass of 1 cm^{-1}.

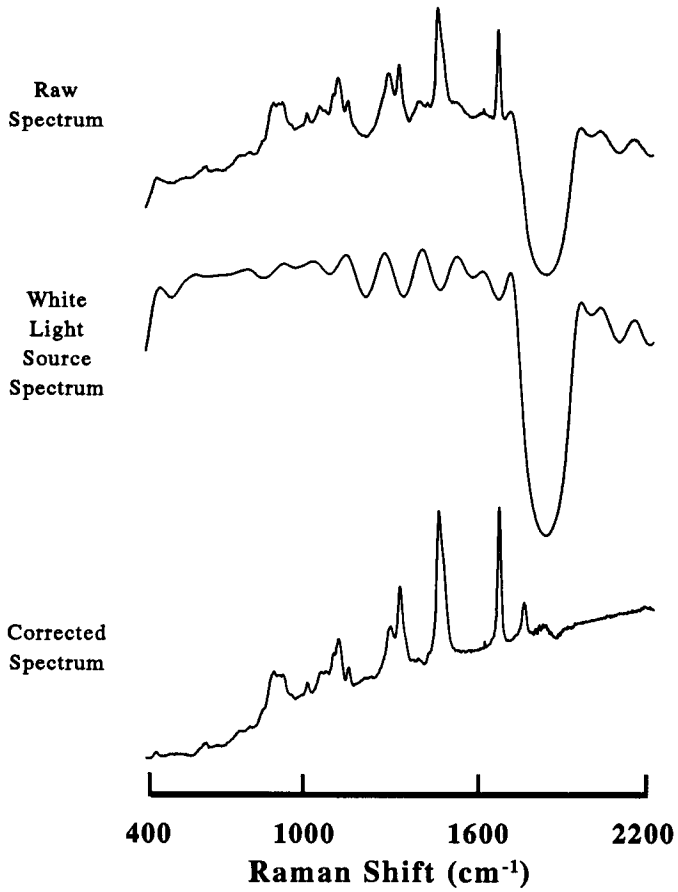

FIG. 7. Raman spectra of oleic acid methyl ester, obtained at 691 nm with a Ti:sapphire laser and Omega REFLP702 filter between the sample and spectrometer. The corrected spectrum was obtained as described in the text, via Eq. 19.

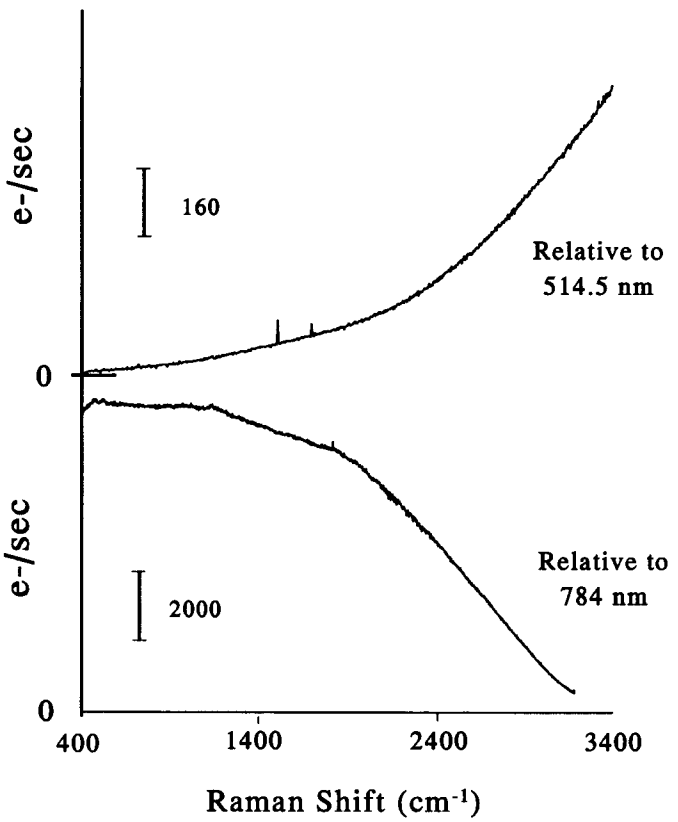

FIG. 8. Raw spectra of white fiber source obtained with spectrometer C. The x-axis is plotted as Raman shift relative to the laser wavelength indicated. The spikes on upper spectrum are random hard radiation events.

then multiplying by A_D for a given resolution. The observed $\Omega Q T A_D$ function is plotted as a function of wavelength for several spectrometers in Fig. 6. For these comparisons, the bandpass used to determine A_D for the Raman experiment was arbitrarily set at 1 cm^{-1}. Note that Fig. 6 does not take any multichannel advantage into account, but does compare spectrometers for light collection at fixed spectral resolution.

To correct observed Raman intensities for instrumental response, it is necessary only to divide the raw spectrum by the instrumental response of the appropriate wavelength range. In practice, the white output from the fiber (S_F) is recorded under the same conditions as the raw spectrum (S_{obs}); then the corrected spectra are calculated from Eq. 19:

$$S_{corr} = \frac{S_{obs}}{S_F} L_F. \tag{19}$$

This process is a simple computer operation once L_F is known.

The raw spectrum shown in Fig. 7 is perturbed by the structure in the laser rejection filter, to the point where the spectral information is obscured. When the raw spectrum is multiplied by L_F/S_F from a white light spectrum obtained under the same conditions, these artifacts are removed.

An equally important but less commonly appreciated consequence of instrumental response is distortion of relative peak intensities. Figure 8 shows the white light response from spectrometer **C**, but replotted in terms of Raman shift from two common laser wavelengths. For an Ar^+ laser, the larger Raman shifts (e.g., C-H stretch) will be enhanced, while for a Ti:sapphire laser at 784 nm, they will be suppressed. This effect is shown in Figs. 9 and 10 for spectra of methylene chloride and naphthalene. In both cases, the raw spectra were corrected by multiplying by L_F/S_F recorded under identical conditions.

DISCUSSION

Although continuum source sensitivity calibration is not new, the current discussion in the context of CCD detectors provides two useful observations. First, an accurate white light calibration corrects the spectrum for distortion of relative peak intensities caused by T and Q variations with wavelength. This correction is more accurate when the white source is placed at the Raman sample position, since it will then correct for chromatic and off-axis aberrations of the collection optics and other components. Hamaguchi has discussed the use of a fluorophore with known fluorescence intensity (quinine) as a source of continuum emission for sensitivity calibration.[19] This approach will precisely reproduce Raman scattering conditions, and will avoid any uncertainty in positioning of the white light fiber. However, it only ap-

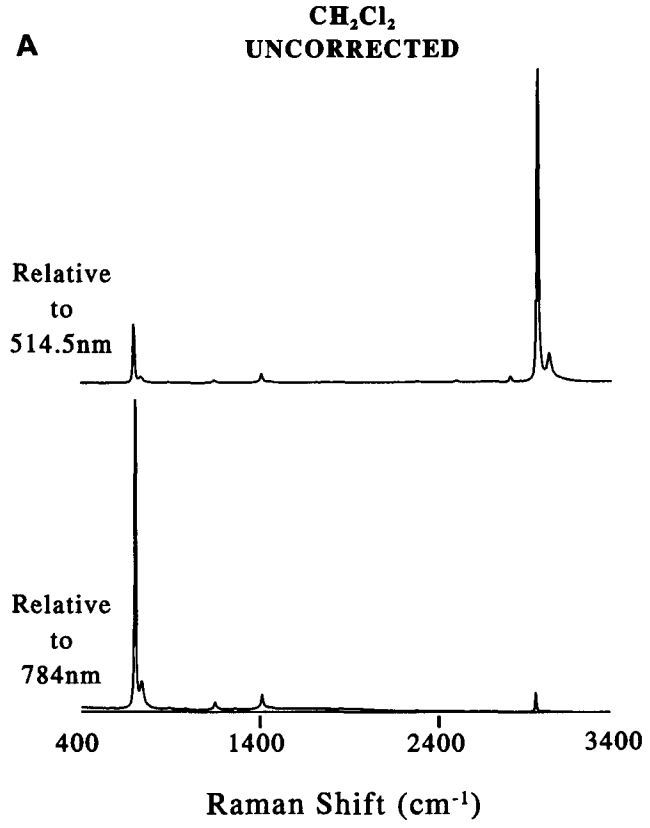

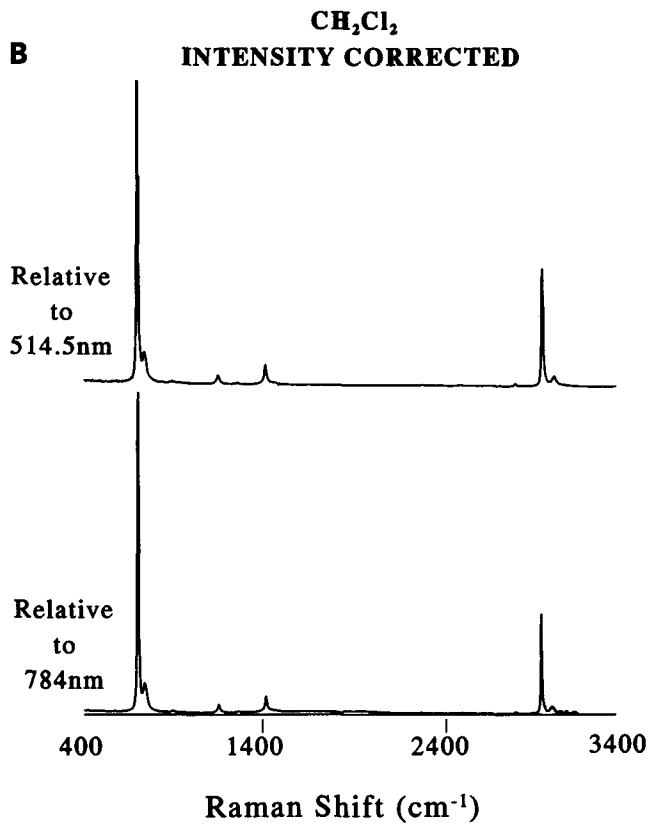

FIG. 9. Spectra of methylene chloride obtained with 514.5- and 784.0-nm lasers before (**A**) and after (**B**) white light correction via Eq. 19.

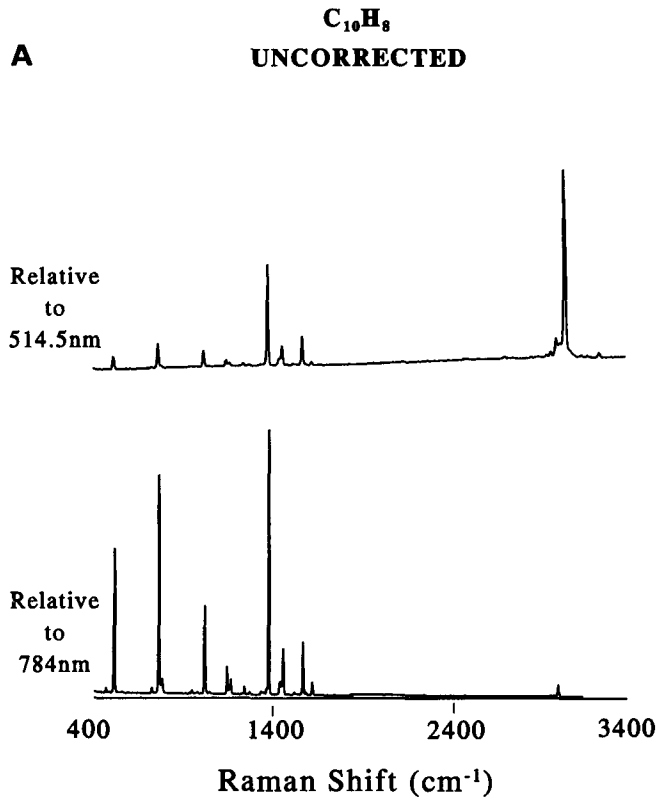

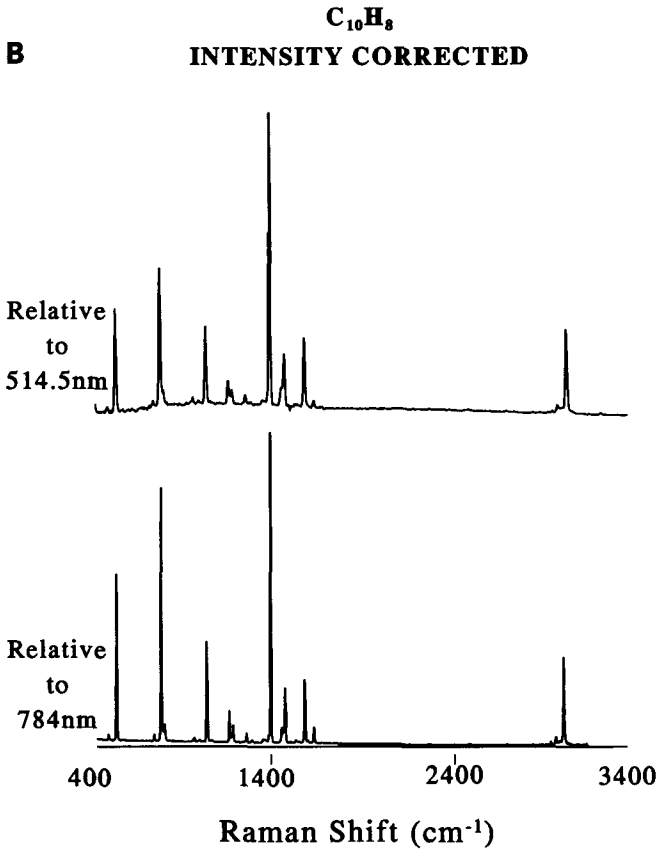

FIG. 10. Spectra of napthalene; same conditions as Fig. 9.

plies to a limited spectral range (400–600 nm) and requires a UV laser. In principle, one could establish several fluorophores covering the entire range of interest (up to 1100 nm), but a simple tungsten source is currently available that covers the entire 400–1100 nm range. Application of the white light correction to the removal of spectral artifacts is shown in Figs. 9 and 10. Although an analogous correction is common in FT-IR and FT-Raman, it is not yet common in dispersive Raman.

Correction for instrumental response is particularly important when one is using CCDs and NIR lasers due to the quite different $Q(\lambda)$ response of CCDs compared to PMTs. As shown in Fig. 8, the increase in Q over the 3000-cm^{-1} Raman shift range relative to 514.5 nm, as well as the decrease over the same range relative to 784 nm, leads to the very different intensity profiles apparent in the uncorrected spectra of Figs. 9 and 10. The white light correction effectively removes this instrumental distortion, to the extent permitted by noise level. The slightly more intense (1382-cm^{-1}) band of naphthalene observed for a 514.5-nm laser after correction is likely to be due to preresonance of the ring breathing mode. The increased noise level in the corrected spectra at 3000 cm^{-1} relative to 784 is due to the low Q of the CCD in this region.

A second important consequence of the white light calibration is assessment of spectrometer performance. The shape of the ΩQTA_D curve reveals relative sensitivity for different laser wavelengths or for different diffraction gratings (Fig. 6). In addition, the constancy of L_F when the fiber is moved among several spectrometers or different configurations of a given spectrometer allows a quantitative comparison of sensitivity. In particular, comparison of the relative ΩQTA_D product provides assessment of the spectrometer figure of merit (Eq. 14). On the basis of Eq. 14, a higher value of this product yields a higher signal for a given sample power density and time. Similarly, the SNR scales with $(\Omega QTA_D)^{1/2}$, all else being equal. Relative F_s values are listed in Table I for two wavelengths. These observations have several obvious but useful consequences dealing with S and SNR. First, S is proportional to $\beta_a D_a$, so an increase in cross section permits a proportional decrease in D_a (or concentration) to yield a given signal. Second, lower $\beta_a D_a$ requires higher P_D or longer t to yield the same S (or SNR). The larger the right side of Eq. 18, the lower β_a, D_a, P_D, or t can be to achieve the same S. The same statement applies to SNR via Eq. 15. Small $\beta_a D_a P_D t$ can be compensated by N_R to keep the SNR constant. Furthermore, if F_{SNR} is known, one can use Eq. 15 to predict how large the $(\beta_a D_a P_D t)$ product must be to achieve a desired SNR. Equations 14 and 15 are essentially quantitative statements of the trade-offs of cross section, concentration, N_R, P_D, etc., which are often encountered in a Raman experiment. Recall that F_{SNR} takes into account the Ω, A_D, T, and Q of a particular spectrometer for a given resolution, but does *not* incorporate spectral coverage or any multichannel advantage.

The response curves of Fig. 6 reveal several points about spectrometer performance. First, the increase in response for the higher T, Ω, and Q of spectrograph **B** compared to system **A** is not as great as expected, due to the small pixel area, in comparison with that for a PMT. The large PMT area permits $f/$ matching in system **A**, partially compensating for its large $f/$. While system **B** will still exhibit a multichannel advantage, the gain will not be as high as expected if all else is equal. Second, the discontinuities in curves **B**, **C**, and **D** are common for multiple-segment CCD acquisitions, and are apparently due to variations in throughput for light focused at various points on the CCD surface. They are reproducible and are correctable with the white light calibration. Third, a lower $f/$ spectrograph and higher Q detector lead to substantial improvements in sensitivity and SNR. The factor-of-four increase in response for system **D** over **C** is due to increased Ω [which scales inversely with the square of $f/$, in this case $(5.6/4.0)^2$] and an increase in Q of a factor of about two at 700 nm. The response above 900 nm for **D** vs. **C** is greater than a factor-of-four larger due to the enhanced red response of back-thinned CCDs. The oscillation in response for system **D** above 750 nm is apparently due to interference effects in the CCD. The oscillations are correctible with the white fiber source provided that both the sample and white source fully illuminate the CCD height.

While the white light calibration is useful for spectrometer comparisons, the long-term value of the approach may lie in intensity correction of Raman spectra. Published spectra are not commonly corrected for instrument response at present, but reliable relative intensities are quite valuable for spectral searches, qualitative analysis, and cross section comparisons. The white light correction is most accurate when the known white source most accurately reproduces the scattering geometry of the Raman samples.

ACKNOWLEDGMENT

This work was supported by the Analytical and Surface Chemistry Division of the National Science Foundation.

1. A. Campion, J. Brown, and W. H. Grizzle, Surf. Sci. **115,** L153 (1982).
2. A. Campion and W. H. Woodruff, Anal. Chem. **59,** 1301A (1987).
3. C. A. Murray and S. B. Dierker, J. Opt. Soc. Am. **3,** 2151 (1986).
4. S. B. Dierker, C. A. Murray, J. D. LeGrange, and N. E. Schlotter, Chem. Phys. Lett. **137,** 453 (1987).
5. J. Pemberton and R. Sobocinski, J. Am. Chem. Soc. **111,** 432 (1989).
6. J. Pemberton and R. Sobocinski, Appl. Spectrosc. **44,** 328 (1990).
7. R. T. Packard and R. L. McCreery, Anal. Chem. **59,** 2631 (1987).
8. R. T. Packard and R. L. McCreery, Anal. Chem. **61,** 775A (1989).
9. A. Campion and S. Perry, Laser Focus World, **August,** 113 (1990).
10. P. M. Epperson, J. V. Sweedler, R. B. Bilhorn, G. R. Sims, and M. B. Denton, Anal. Chem. **60,** 327A (1988).
11. J. J. Freeman, J. Heaviside, P. J. Hendra, J. Prior, and E. S. Reid, Appl. Spectrosc. **35,** 196 (1981).
12. R. L. McCreery, in *Charge Transfer Devices in Chemistry,* J. Sweedler, K. Ratzlaff, and M. Denton, Eds. (VCH, New York, in press).
13. J. M. Williamson, R. J. Bowling, and R. L. McCreery, Appl. Spectrosc. **43,** 372 (1989).
14. Y. Wang and R. McCreery, Anal. Chem. **62,** 2647 (1989).
15. C. D. Allred and R. L. McCreery, Appl. Spectrosc. **44,** 1229 (1990).
16. T. D. Harris, M. L. Schnoes, and L. Seibles, Anal. Chem. **61,** 994 (1989).
17. C. D. Newman, G. G. Bret, and R. L. McCreery, Appl. Spectrosc. **46,** 262 (1992).
18. C. Shen, T. J. Vickers, and C. K. Mann, Appl. Spectrosc. **46,** 772 (1992).
19. H. Hamaguchi, Appl. Spectrosc. Rev. **24,** 137 (1988).
20. M. Pelletier and R. Reeder, Appl. Spectrosc. **45,** 765 (1991).

21. B. Schrader, A. Hoffman, A. Simon, and J. Sawatzki, Vibrational Spectrom. **1,** 239 (1991).
22. B. Schrader, A. Hoffman, and S. Keller, Spectrochim. Acta **47A,** 1135 (1991).
23. S. D. Schwab, R. L. McCreery, and F. T. Gamble, Anal. Chem. **58,** 2486 (1986).
24. S. Asher, Anal. Chem. **65,** 59A (1993).
25. D. L. Long, *Raman Spectroscopy* (McGraw-Hill, New York, 1977).
26. C. D. Allenmand. Appl. Chem. **65,** 59A (1993).
27. R. L. Schweisow, J. Opt. Soc. Amer. **59,** 10 (1969).
28. R. P. Van Duyne, in *Chemical and Biological Applications of Lasers,* L. B. Moore, Ed. (Academic Press, New York, 1979), Vol. 4, Chap. 4.
29. D. Strommen and K. Nakamoto, *Laboratory Raman Spectroscopy* (Wiley, New York, 1984).